Am J Transl Res 2022;14(11):7792-7805
www.ajtr.org /ISSN:1943-8141/AJTR0144209

Original Article

A novel classification based on non-apoptosis cell death predicts clinical outcomes and immunotherapy response of clear renal cell carcinoma

Liuxun Chen[2], Xvdong Liu[1], Shenjie Zeng[1], Huimin Zhu[1], Jiawu Wang[2], Qing Jiang[2]

[1]First Clinical Institution, Chongqing Medical University, Chongqing, China; [2]Department of Urology, The Second Affiliated Hospital of Chongqing Medical University, Chongqing, China

Received May 17, 2022; Accepted September 26, 2022; Epub November 15, 2022; Published November 30, 2022

Abstract: Background: Non-apoptosis cell death could be a secondary consequence of the immune response, which profoundly influences tumor microenvironment (TME), escaping from chemotherapy/immunotherapy-induced apoptosis resistance effects. Whereas, systemic analysis of non-apoptosis regulated cell death associated with TME and clinical outcomes remains unveiled. Methods: Our kidney clear carcinoma (KIRC) samples from The Cancer Genome Atlas (TCGA) were stratified into three clusters based on the activity of autophagic cell death, ferroptosis, pyroptosis and necroptosis. Clinical prognosis, TME landscape, biological functions and somatic mutation frequency were compared among the clusters. Additionally, to identify a gene signature highly correlated with clinical prognosis, a risk score model was constructed, and the clinical prognosis, immune infiltration, somatic mutation and biological pathways of risk score subgroups were investigated. Results: Our non-apoptosis cell death clusters are robustly predictive of immunotherapy responses. Patients in Cluster B are the most sensitive to immune checkpoint blockades-depended immunotherapy. Our risk score model was also verified as a promising biomarker for clinical prognosis and immunotherapy efficiency. Where, the High-risk score group was more sensitive to immunotherapy. Conclusions: The novel non-apoptosis cell death-based classification and risk score model could predict the outcome of immunotherapy, and highly associate with immune infiltration. These findings may provide a novel strategy to aid in identificatin of biomarkers and selecting personalized therapeutic strategies.

Keywords: Autophagic cell death, ferroptosis, pyroptosis, necroptosis, tumor microenvironment, immunotherapy

Introduction

Precision medicine and personalized treatment have eased the outlook of many patients diagnosed with advanced cancers. The basic purpose of precision medicine is to match a suitable drug with the suitable patient by targeting the specific molecules [1]. Renal cell cancer (RCC) originates from the nephron tubules, and comprises a heterogeneous group of cancers. The most common subtypes are kidney renal clear cell carcinoma (KIRC), accounting for 70%-75% of cases [2]. More and more studies identified effective biomarkers, which were restricted by intratumoral heterogeneity. Recently, insights obtained from the molecular characterization of aberrant genes and signaling pathways associated with tumors have been incorporated into clinical strategies. Predictably, a more extensive evaluation of the high-resolution molecular data, containing abundant clinical data, and therapy details, should reduce the gaps in our understanding of cancer biology and pave the way for improving cancer treatments [3]. However, thousands of parameters provided by transcriptome cover too much information which are overwhelming and unsustainable for routine treatment decisions [4].

The tumor immune microenvironment (TME) is a complex ecosystem that plays a critical role in cancer progression and response to therapy [5]. More and more experimental evidence suggests the interplay of ferroptosis, necroptosis, or pyroptosis with tumor immunity. Tumor cells that undergo regulated cell death may trigger robust antitumor immunity, and combination

therapy of cell death inducers and immune checkpoint inhibitors (ICIs) may exert a synergistic and promising role in enhancing antitumor activity [6, 7]. Additionally, autophagic cell death independent from of ferroptosis, necroptosis and pyroptosis, occurs in a subpopulation of cells that undergo the highest levels of autophagy during nutrient starvation [8]. Furthermore, autophagic cell death's crosstalk with other regulated cell death has been widely reported recently, which notably influencing and even reshaping TME [9]. Therefore, the activation of the aforementioned cell death may help eliminate the cancer cell, which is pivotal for the occurrence and development of tumors. Nevertheless, comprehensive and integrated transcriptome analyses that access the non-apoptosis cell death including *autophagic cell death, ferroptosis, pyroptosis and necroptosis* remain unreported. Here, we developed a novel method for classifying of KIRC samples into three TME clusters with notably distinct immune infiltration and clinical outcomes. Then, we systematically evaluated our novel classification's immune response's predictive efficacy. Additionally, a risk score model was constructed based on the differentially expressed genes among the TME clusters; the model is associated with clinical prognosis and immunotherapy response of KIRC. Altogether the classification system could help dissect a unique TME characterization of KIRC and to interpret the clinical responses to immunotherapies, providing new molecules beneficial for the diagnosing and treating of cancers.

Methods

Data download and processing

Autophagic cell death, ferroptosis, pyroptosis and *necroptosis* related genes were obtained from the Molecular Signatures Database (MsigDB, https://www.gsea-msigdb.org/gsea/msigdb/) [10] including "GOBP_AU-TOPHAGIC_CELL_DEATH", "WP_FERROPTOSIS", "REACTOME_PYROPTOSIS" and "GOB-P_NECROPTOTIC_SIGNALING_PATHWAY", and signatures of 28 immune cells were all from G Bindea, B Mlecnik et al (Table S1) [11]. The FPKM values of genome expression files (n=539) and the somatic mutation data of kidney renal clear cell carcinoma (KIRC) and normal renal tissue were downloaded from The Cancer Genome Atlas (TCGA, https://portal.gdc.cancer.gov/), where corresponding clinical information was incorporated. Two KIRC validated cohorts (GSE53757 n=144, GSE73731 n=256) were obtained from Gene-Expression Omnibus (GEO). The fragments per kilobase of exon per million mapped (FPKM) format of genome expression values was then transformed into the format of transcript per million (TPM). The "maftools" R package was applied to process the mutation annotation format (maf) data. The study did not require the approval from the ethics committees because all data were open-access in the TCGA or GEO database.

Tumor-infiltrating cells and abundance of autophagic cell death, ferroptosis, pyroptosis, and necroptosis analysis

Single-sample gene set enrichment analysis (ssGSEA) is an extension of Gene Set Enrichment Analysis (GSEA), which calculates enrichment scores for the gene set [12]. To better elucidate the abundance of regulated cell death containing *autophagic cell death, ferroptosis, pyroptosis and necroptosis*, and immune infiltrating cells, we used the "GSVA" R package to apply the ssGSEA algorithm to determine the enrichment scores.

Unsupervised clustering

Unsupervised clustering algorithm was applied to obtain different clusters based on the ssGSEA enrichment scores. Package "ConsensuClusterplus" was used to perform this step and to the number of clusters and ensured the stability of the classification.

Annotation and pathway enrichment analysis

Gene Ontology (GO) analysis were conducted using the "clusterProfiler" R package to determine the downstream biological processes, cell components, and molecular function pathways. Furthermore, GSEA analysis was performed using gsea-3.0 software to investigate the enrichment pathways of differentially expressed genes (DEGs). p-value < 0.05 and adjusted p-value (Q value) < 0.05 were considered statistically significant.

Evaluation of immune infiltration, TMEscore and tumor mutation burden

To precisely dissect the features of the KIRC tumor immune microenvironment, in the begin-

ning, we compared the expression levels of immune checkpoints (PD-1, CTLA-4, LAG-3, and TIM-3) in the different clusters using Kruskal-Wallis' test and applied Pearson's correlation analysis to identify genes associated with immune checkpoints. To further address the mechanisms regulating the expression of these immune checkpoints, Pearson's correlation algorithm was conducted to evaluate the relationship between the expression levels of immune checkpoints and activity of the pathways including IFN-α, β pathway, TGF-β pathway, hypoxia pathway, TNF-α related pathway, IL-2 related pathway, and WNT/β-catenin pathway. All above signaling pathways modulated the expression of the aforementioned immune checkpoints [13], and all the signature genes of the above pathways were also acquired from MsigDB. Afterward, the Estimation of STromal and Immune cells in Malignant Tumors using Expression data (ESTIMATE) algorithm was adopted to calculate the stromal and immune scores. TMEscore, which is considered a helpful tool to predict tumor immunogenicity and ICIs sensitiveness from bulk transcriptomic data [14] was adopted to investigate the comprehensive features of TME. Additionally, to obtain the tumor mutational burden (TMB), we counted the nonsynonymous and synonymous mutation counts of each patient in the TCGA-KIRC cohort.

Differentially expressed gene analysis

Package "limma" applied to screen out the differently expressed genes (DEGs) among the phenotypes using the Chi-Squared test. We intersected the DEGs and genes with different expressions in bladder cancer tissue comparing normal tissue based on TCGA cohorts. Considering the least absolute shrinkage (LASSO), univariant and multivariant cox regression analysis were successively performed using the R package "glmnet" to select candidate genes for constructing the risk model, riskscore = (coefi × Expi), where i refers to the number of selected DEGs.

Identification of clinical significance of riskscore

The samples were divided into low- and high-riskscore groups, where the cut-off was set at the median of these scores. We applied package "survival" to evaluate the difference of overall survival between the categorized patients. To estimate the predictive capability of riskscores, univariate and multivariate cox regression analyses were used followingly. Subsequently, a difference analysis of riskscores was performed with clinicopathological features using Kruskal-Wallis' test (clinical stage, T, M, N stage, and pathological grade). And the correlations of riskscores with clinical stages, M and N stages, were then verified by samples from the GEO database. Lastly, the areas under the curve (AUC) of the receiver operating characteristic (ROC) curve were applied to evaluate the predictive value of gene signature. Subsequently, we correlated the selected genes' constructed riskscores and expression levels with the ssGSEA scores of the regulated cell death (*Autophagic cell death, ferroptosis, pyroptosis* and *necroptosis*). KIRC samples in various clinical stages to conduct correlation analysis to investigate the relevance of the expression of selected genes and Stromal and Immune scores computed by the ESTIMATE package to explore how selected genes influence the immune infiltration in KIRC patients at different disease stages.

Statistical analysis

Data analyses and visualization were mainly completed by R (version 4.0.3) software, PERL 212 programming language (version 5.32.1.1). Statistical significance for normally distributed variables was estimated by unpaired wilcox tests for comparisons of two groups. The Kaplan-Meier Technique was used to generate survival curves. *p*-values of less than 0.05 were considered statistically significant.

Results

Non-apoptosis regulated cell death clusters exhibit different clinical prognosis and immune infiltration

Based on ssGSEA scores of immune infiltration, *pyroptosis, autophagy, ferroptosis, and necroptosis*, unsupervised clustering was implemented and accessed three clusters, that were ultimately obtained, were accessed including 305 samples in Cluster A and 165 samples in Cluster B, 60 samples in Cluster C. The Cluster B was characterized as high-enrichment inflammation, while Clusters A and C were characterized as middle-enrichment and

low-enrichment, respectively (**Figure 1A**). The boxplot also showed a significant difference between infiltration and non-apoptosis regulated cell death enrichment in the clusters (**Figure 1B**). Additionally, the patients in Cluster A had significantly longer overall survival (OS) compared with patients in Clusters B and C (**Figure 1C**, P=0.04). Generally, high activation of non-regulated cell death is probably accompanied by high immune infiltration and vice versa. Furthermore, this corresponding relationship also affects the clinical survival of KIRC patients.

Non-apoptosis regulated cell death clusters predict distinct immunotherapy efficiency

According to the different immune infiltration phenotypes, it was speculated that Cluster B could respond to immunotherapy the most, while Cluster C could be the least sensitive. To address these questions, first, the expression of immune checkpoints were compared among the clusters (**Figure 2A-D**). As the targets of ICIs, the expression of immune checkpoint molecules could essentially predict the effect of ICBs. Intriguingly, the results showed that the expression of PD1, CTLA4, LAG3, and TIM3 were upregulated in Cluster B, and downregulated in Cluster C, which prompted me to explore further the biological mechanisms that induced the upregulation of these immune checkpoints. To show the heterogeneity in the expression of immune checkpoints in Cluster B patients. The unsupervised clustering algorithm was applied to divide Cluster B patients into two subclasses further: B1, and B2 (Figure S1A). As expected, the heatmap suggested a notably different expression of these immune checkpoints between Clusters B1 and B2 (Figure S1B). Subsequently, the signature genes of pathways that were widely reported to potentiate in regulating the expression of PD1, CTLA4, LAG3 and TIM3 from the molecular signature database. The ssGSEA scores of IFN-α, IFN-β, IL-2, IL-6, and TNF related pathways showed a trend similar to the above immune checkpoint expression (Figure S1C). Additionally, genes highly correlated with immune expression (checkpoints correlation coefficient > 0.35, P < 0.001), were extracted and GO analyses were performed to identify potential upstream pathways (Figure S1D). The correlation heat map more precisely depicts the statistical relationship between the above upstream pathways and these immune checkpoints (Figure S1E).

Second, the stromal and immune components in TME were further calculated and compared for each sample. Our results showed that the StromalScores and ImmuneScores among the clusters significantly differed (**Figure 2E**, **2F**). Third, the TMEscore for each patient was estimated to predict tumor immunogenicity and ICIs sensitiveness from bulk transcriptomic data (**Figure 2G**). Lastly, previous research underscored that higher TMB was associated with longer survival after treatment with ICIs [14]. Our result showed a significant difference between Clusters A and C, while there was no significant difference from Cluster B (**Figure 2H**). These results suggested that our classification system could predict the immunotherapy response in KIRC patients.

Non-apoptosis regulated cell death clusters exhibit different biological functions

Genomic mutations can act as oncogenic drivers which enable tumorigenesis and promotion. The mutation landscapes of the three different clusters deepen our understanding of their different biological characteristics. The top 20 mutated genes were respectively displayed in the waterfall curve (**Figure 3A-C**). Among them, VHL was the first common mutated gene with 51%, 46%, and 23% mutation rates, respectively. The mutation rates of Polybromo-1 (PBRM1) (47%) in Cluster A were significantly higher than patients in Cluster B (32%), and Cluster C (19%). Additionally, SETD2 mutation rates in Cluster C are ultimately lower (< 6%) than that in Cluster A (12%) and B (15%). Moreover, there are higher mutation variation rates of MTOR (19%) and TP53 (10%) in Cluster C. To further examine the potential upstream and downstream biological behavior of the distinct non-apoptosis cell death clusters, DEGs were screened out (Table S2) after which GO analysis among the three clusters was performed (Table S3). In GO enriched pathways, Cluster A was characterized by the humoral immune response (**Figure 3D**), such as immunoglobulin mediated immune response, complement activation classical pathway. Cluster B was characterized by the enhanced immune-related pathways (**Figure 3E**), such as immune

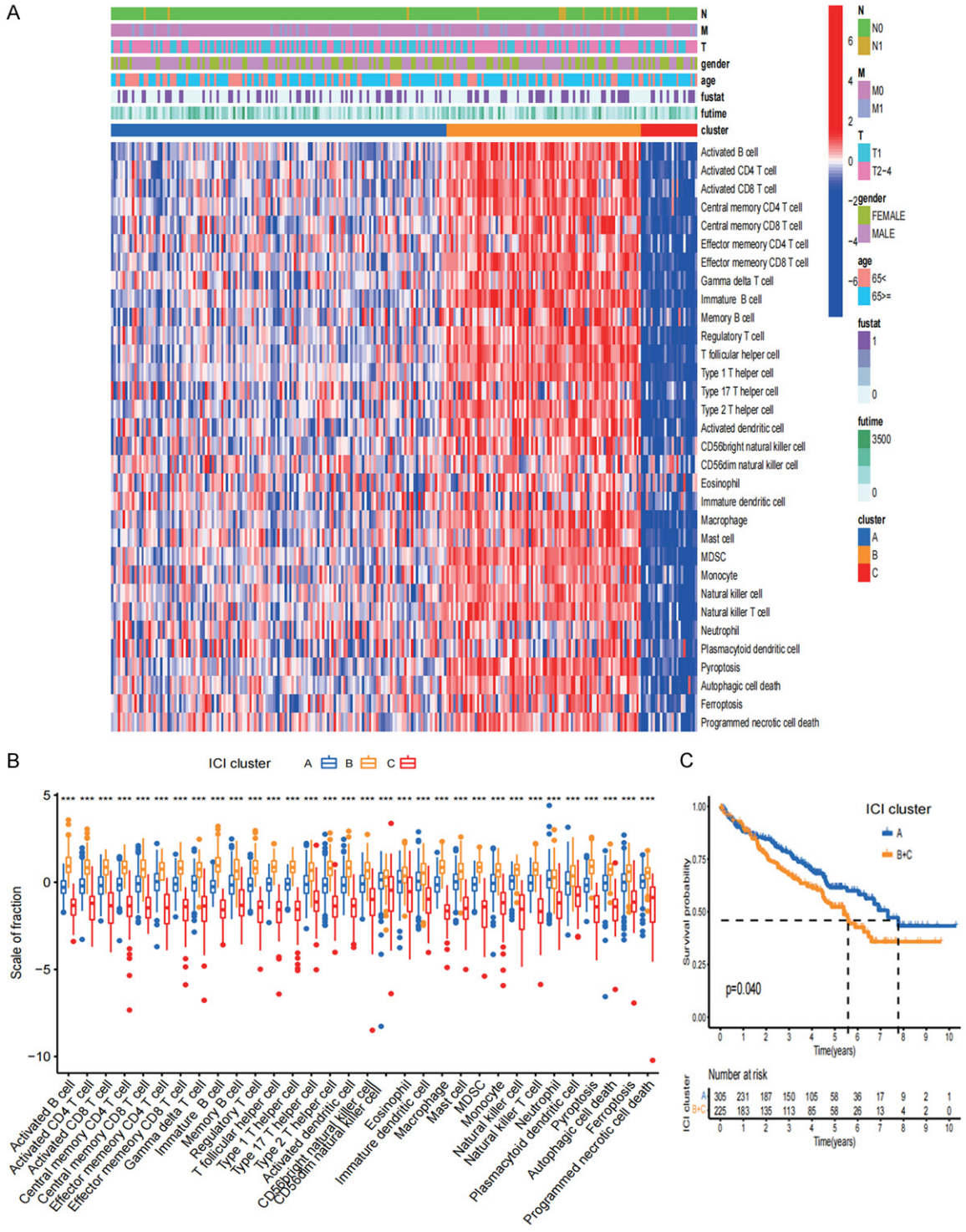

Figure 1. Dramatic distinctions of Tumor microenvironment (TME) features among Cluster A, Cluster B and Cluster C. A. Complex heatmap demonstrated different immune infiltration in Cluster A, B, and C. B. Violin plot showed the alterations among the Clusters in immune cells. C. Kaplan-Meier plot of Kidney Renal clear cell carcinoma (KIRC) patients in the three clusters.

response-activating signal transduction, immune response-activating cell surface receptor signaling pathway, positive regulation of leukocyte activation, production of molecular media-

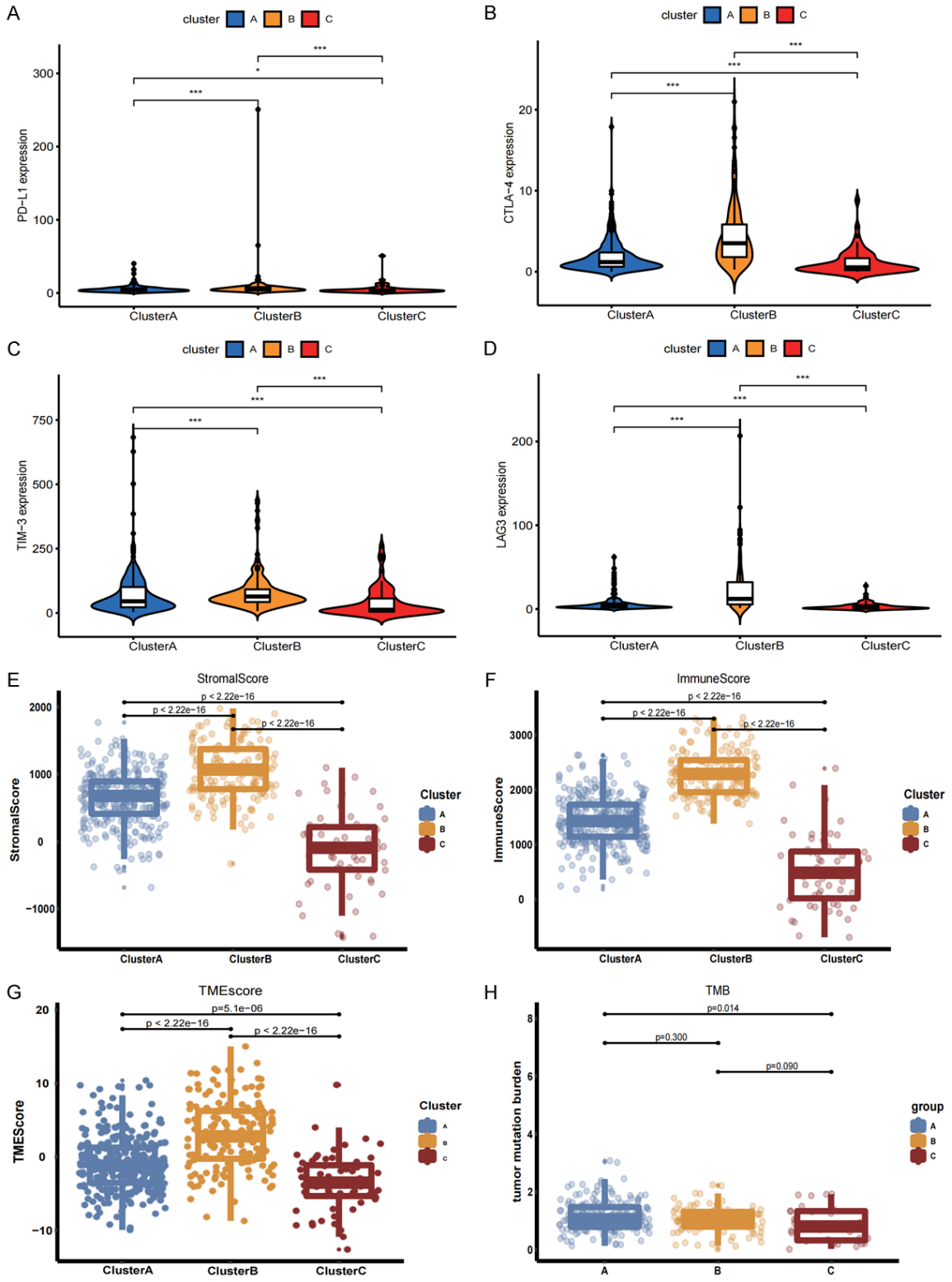

Figure 2. Classification based on cell death could predict the immunotherapy efficacy. Violin plots suggested the different expression of PD-L1 (A), CTLA-4 (B), TIM-3 (C) and LAG-3 (D). Box plots showed that StromalScore (E), ImmuneScore (F), TMEscore (G) and Tumor mutation burden (TMB) (H) were distinct among Clusters A, B and C.

tor of the immune response, and response to interferon-gamma. While, Cluster C was characterized by the upregulated metabolism pathways (**Figure 3F**), such as response to drugs,

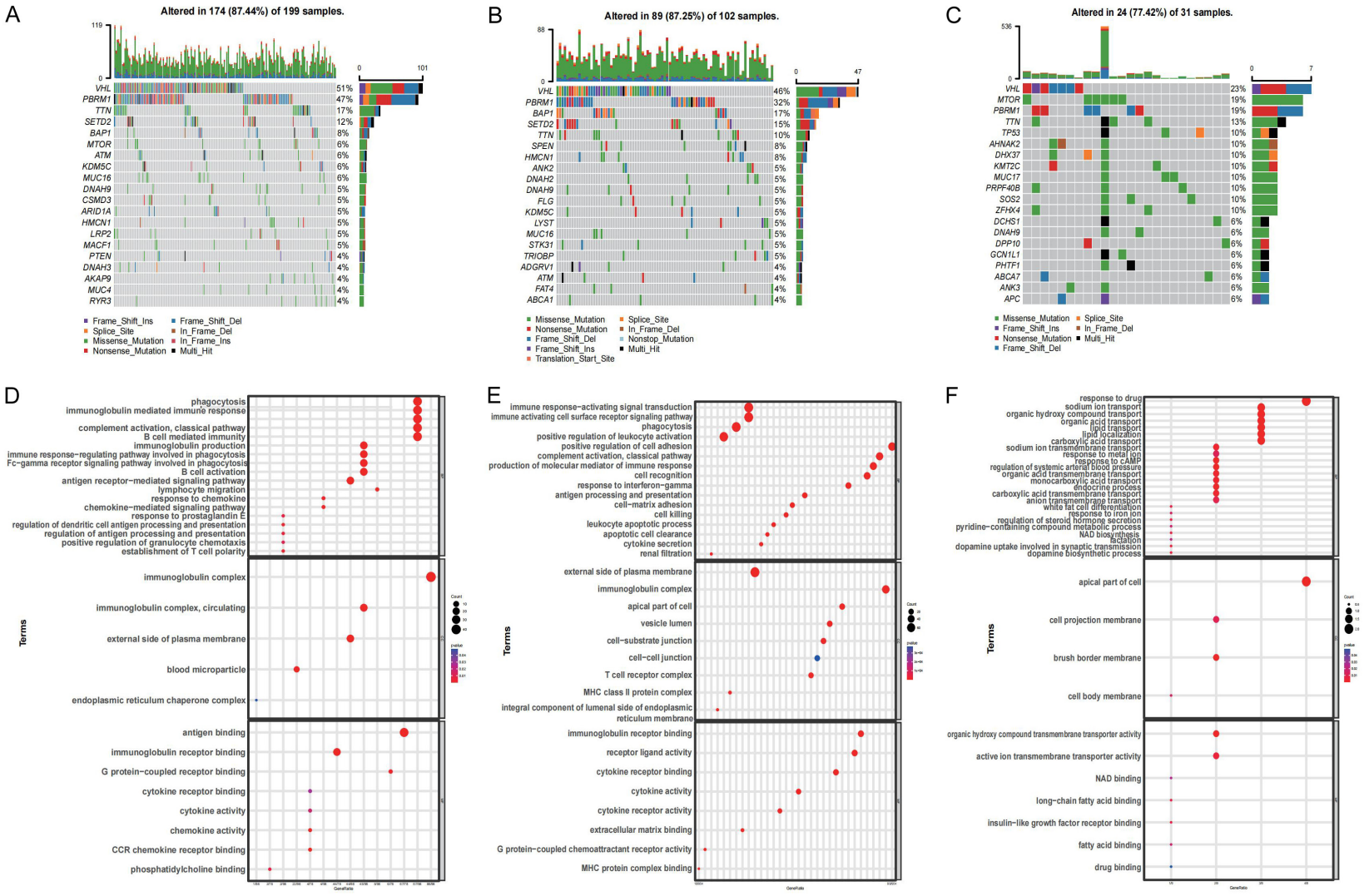

Figure 3. Characteristics of Clusters with somatic mutation, biological function. (A-C) Waterfall plot was depicted to display the somatic mutation of patients in Cluster A (A), B (B) and C (C) respectively, each column displayed the individual KIRC samples, TMB of each sample was exhibited by upper bar diagram. The right number represented the mutation frequency, and the bar diagram on the right exhibited the proportion of each mutation type, including missense, nonsense, splice, frameshift, and multiple mutations. (D-F) Gene Ontology (GO) enrichment analysis of high-expression genes in Cluster A (D), Cluster B (E), and Cluster C (F), respectively.

organic acid transport, and metal ion and anion transmembrane transport. What's more, immune pathways were enriched in Cluster B, which again confirmed that patients in Cluster B could be more sensitive to clinical immunotherapy.

Construction of a riskcore model to estimate individual KIRC sample

Owing to the classification system's unsatisfactory predictive capacity for clinical prognosis, a gene signature that could accurately predict the prognosis of KIRC patients was constructed. Five thousand three hundred and ninety differently expressed genes through pairwise pairing of our Clusters (Table S4). Furthermore, 952 genes that were expressed differently between normal and cancer tissues were selected by taking the intersection with the gene set on GEPIA 2.0 database (Table S5). Additionally, GO and Kyoto Encyclopedia of Genes and Genomes (KEGG) analyses were conducted to indicate the pathways with differential activity in Clusters A, B, and C (Figure S2A, S2B). Then, 15 genes were screened out for subsequent analysis based on LASSO analysis (Figure S3A, S3B), and univariate Cox analysis (Figure S3C). Among these 15 genes, SH3 domain containing 2 (SORBS2), Complement C1r Subcomponent Like (C1RL) and Gamma-Aminobutyric Acid Type B Receptor Subunit 1 (GABBR1), all of which could independently predict the prognosis of KIRC patients, were selected to construct the riskscore model after undergoing the multivariant cox regression (Figure S3D).

Riskscore model can be predictive of KIRC clinical outcomes and immunotherapy efficacy

The capability in prognosis prediction of SORBS2, C1RL and GABBR1 was estimated (Figure S4A-C). Survival analysis suggests that KIRC patients in the low-risk group showed significantly higher OS than those in high-risk group (**Figure 4A**, $P < 0.0001$). Moreover, the univariable cox regression model shows that riskscore, age, tumor grade, T stage, M stage and N stage can affect the prognosis of KIRC patients while the multivariable Cox regression model shows that only risk score and age were the independent predictor of KIRC (**Figure 4B**). Furthermore, (**Figure 4C**) ROC curve was depicted to verify the potential of riskscore model in prediction of g survival at 1, 3, and 5 years (Overall set: AUC at 1-, 3- and 5-year is 0.758, 0.720, and 0.758). Based on the TCGA cohorts, riskscore is positively correlated with clinical stage (P=1.648e-07), grade (P=1.617e-10), T stage (P=6.664e-07), M stage (P=1.958e-06), and N stage (P=0.014) (**Figure 4D**). The riskscore is significantly different between clinical stages of patients by the GSE53757 cohort (P=0.016). Furthermore, our research demonstrated a significant distinction between patients of stage I-III and stage VI by analyzing GSE73731 (P=6.527e-05). Subsequently, the expressions of SORBS2, C1RL and GABBR1, and values of riskscores were correlated with the ssGSEA scores of autophagic cell death, ferroptosis, pyroptosis and necroptosis to evaluate whether they could act as targets for cell death pathways in KIRC, the result showed a significant correlation of the selected genes and the cell death pathways (Figure S4D). To estimate the immunotherapy efficacy, the StromalScore (**Figure 4E**), ImmuneScore (**Figure 4F**), and TMEscore (**Figure 4G**), which helped us access the TME status, were calculated. These results indicate that the high-riskscore group may be more sensitive to immunotherapy. Because of the tumor heterogeneity in patients at different clinical stages, the correlation of SORBS2, C1RL and GABBR1 with immune infiltration were analyzed using the samples from stages I to IV, respectively (Figure S4E). The results suggested that SORBS2, C1RL, and GABBR1 have different patterns of gene-cell regulation in the onset, progression, and end stages of the KIRC. Presumably, our research elucidates that riskscore we calculated could assist clinicians in evaluating the patient's disease state and selecting the appropriate treatment for the patient.

The potential biological functions of SORBS2, C1RL and GABBR1

We next listed the distributions of the top 20 somatic mutant genes with highest frequency, mutation frequency of PBRM1 is identified to be significantly different between high-riskscore and low-riskscore groups (**Figure 5A**, **5B**). Lastly, according to GSEA analysis, the common pathways of the candidate genes are mainly enriched in the GSEA terms "GLYCEROLIPID_METABOLISM", "MAPK_SIGNALING PATHWAY", "MTOR_SIGNALING_PATHWAY", "PHOSPHATI-DYLINOSITOL_SIGNALING_SYSTEM", and "PROPANOATE_METABOLISM". Moreover, the significant enrichment of SORBS2 are "JAK_STAT_SIGNALING_PATHWAY" and "P53_SIGNA-LING_PATHWAY" (**Figure 5C**). C1RL is

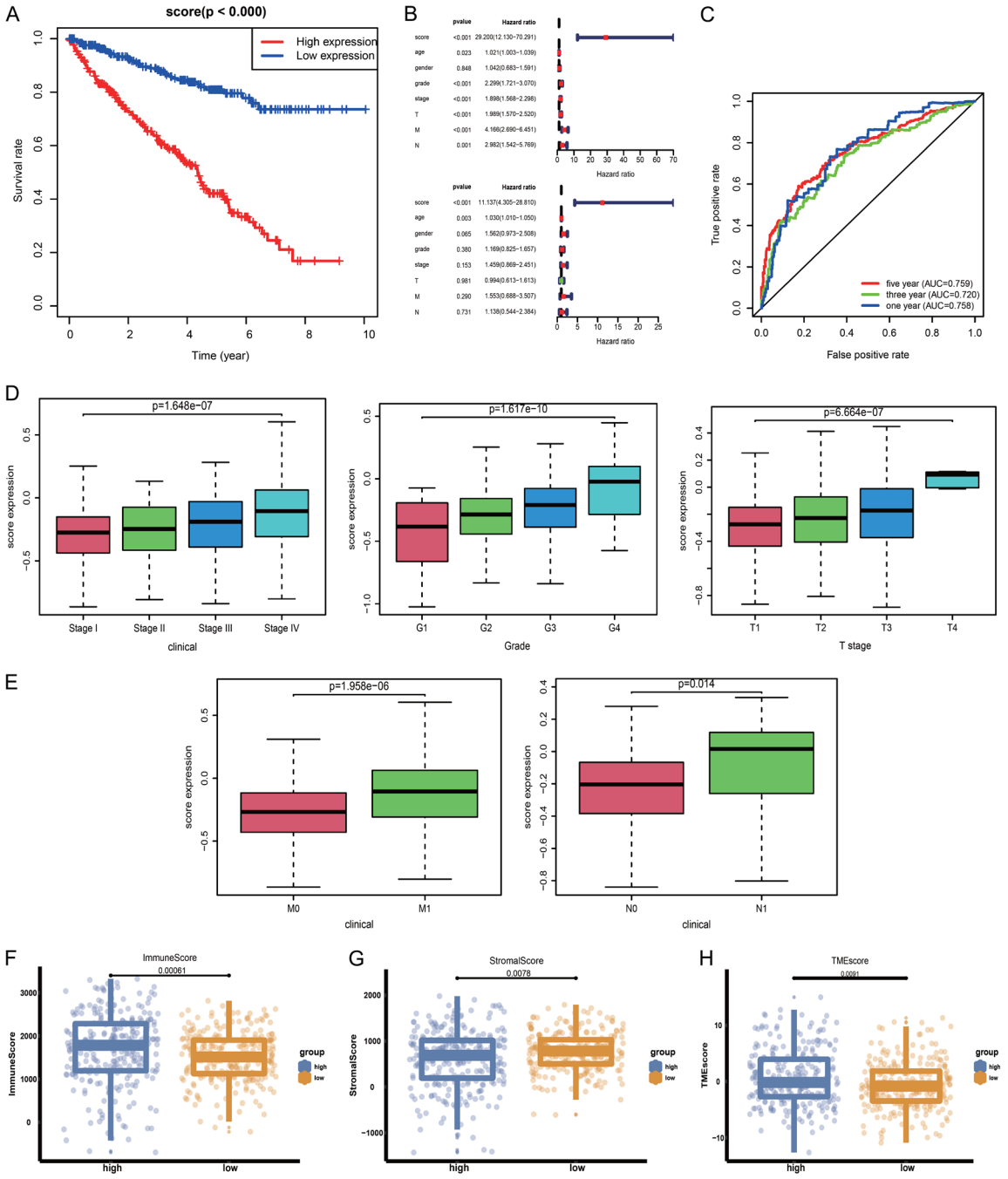

Figure 4. Clinical significance of riskscore. (A) Kaplan-meier plotter of riskscore based on KIRC samples (B) univariable and multivariable cox regression analysis of riskscore. (C) Receiver operating characteristic (ROC) curve indicated areas under the curve of 1-, 3-, and 5-year Overall Survival (OS). (D) According to the TCGA samples, correlation of riskscore and clinical features, including clinical stage, grade, T stage, M stage; (E) Verification relationship between riskscore and T stage (GSE53757) and grade (GSE73731). (F-H) Differences in StromalScore (F), ImmuneScore (G), TMEscore (H) between high-riskscore, and low-riskscore groups in TCGA. The upper and lower ends of the boxes represented the interquartile range of values. The lines in the boxes represented median value.

significantly enriched in "VEGF_SIGNALING_PATHWAY" (**Figure 5D**). The significantly enriched downstream pathways of GABBR1 associated with cancer are "TGF_BETA_SIGNALING_PATHWAY", "WNT_SIGNALING_PATHWAY" and "PATHWAYS_IN_CANCER" (**Figure 5E**). The above enriched pathways play essential roles in different biological behavior and have pro-

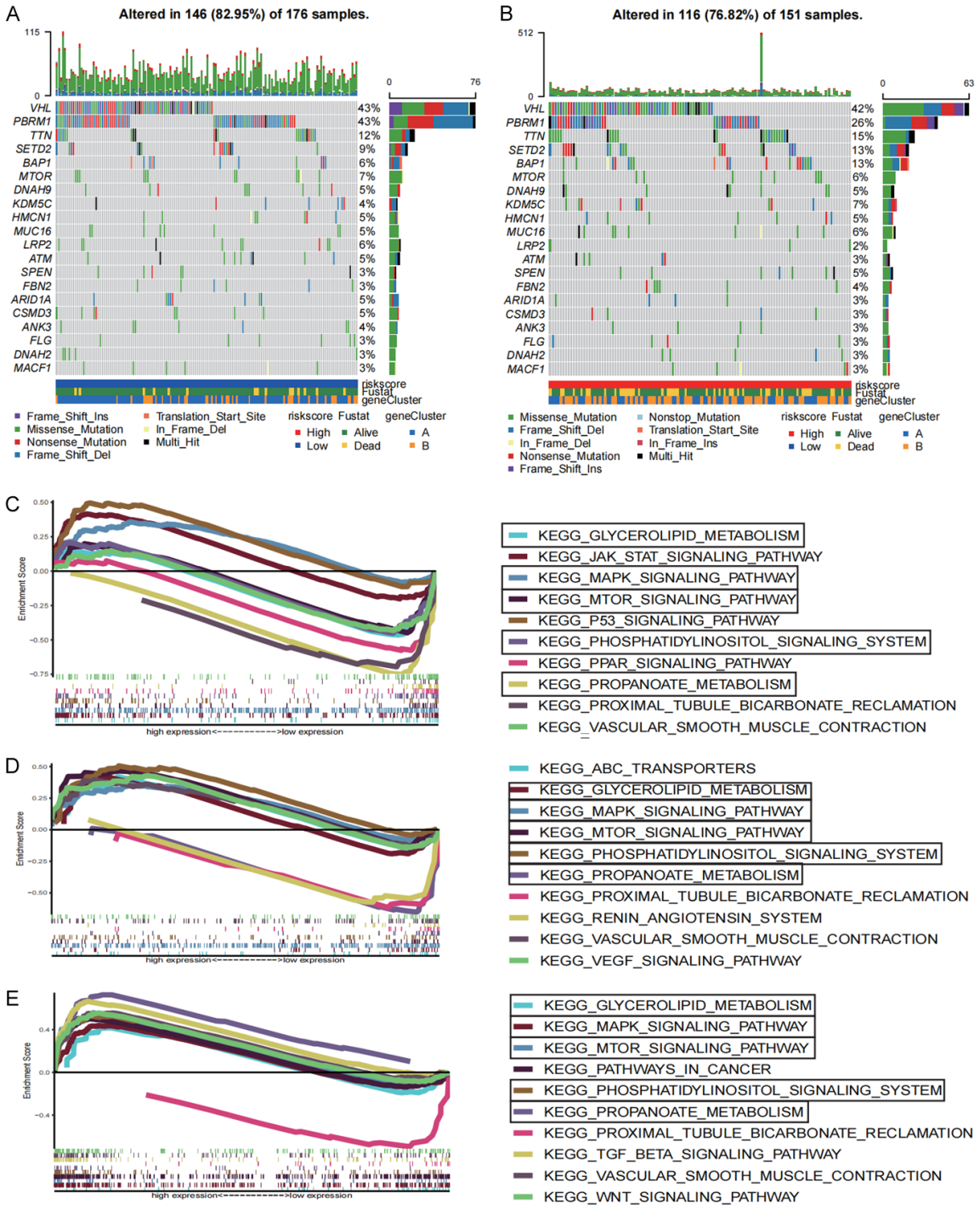

Figure 5. Somatic mutation and GSEA pathways altered in high riskscore group and low riskscore group. (A, B) The waterfall plot of tumor somatic mutation was drawn in those with high riskscore (A) and low riskscore (B) group. (C-E) GSEA of C1RL, GABBR1 and SORBS2, marked by squares are the common pathway of the three pathways.

found effects on the tumor microenvironment. The above findings collectively elucidated that SORBS2, C1RL and GABBR1 could be non-negligible as regards participating in TME formation and KIRC evolution.

Discussion

Implementing precision medicine hinges on integration omics data, including transcriptomics, into the clinical decision-making pro-

cess. A systemic analysis of transcriptomics efficiently contributes to early diagnosis, identification of clinical targets and evaluation of therapeutic efficacy. While one of the translational problems of precision oncology is partly related to the biological heterogeneity of the disease. Recent discoveries have shaped the concept that failure to induce regulated cell death (RCD) is a crucial feature of the tumorigenic process, causing the establishment of various therapeutic strategies [15]. The concept of RCD was continuously expanded after the discovery of a series of novel formation of regulated cell death, such as ferroptosis, pyroptosis, necroptosis and autophagic cell death. Recently, a wealth of evidence suggested that non-apoptosis RCD profoundly alters TME of KIRC and confers different clinical prognoses. Hence, the ssGSEA scores of non-apoptosis RCD were used for classification, and they were correlated with immune infiltration, which was suggestive of three different states of the tumor microenvironment with different clinical prognoses and sensitivity to immunotherapy. Hereafter, a riskscore model was constructed with clinical significance evaluated using TCGA and further verified by GSE5375 and GSE7373 respectively.

Various immune markers that can be used to characterize the tumor's immune status exist. Besides immune cells, cell surface structures, cytokines, and tumor genetics or the microbiome may be used [16]. It was found that the activation of ferroptosis, pyroptosis, necroptosis and autophagic cell death could accurately predict inflammation status. More and more recent studies have also provided evidence that cell death could act as a potent trigger of inflammation, suggesting that cell death could contribute to the pathogenesis of inflammatory diseases and tumors [17-19]. Our enrichment analysis also showed the intrinsic biological connection between cell death and tumor immune, which is particularly involved with lipid metabolism and cell surface and cytokines-related pathways. Additionally, different clusters showed different genomic backgrounds. KIRC has several secondary mutations, including Polybromo-1 (PBRM1) or BAF180, SET domain containing 2 (SETD2), and BRCA1 associated protein 1 (BAP1) [20]. Our research may provide a clue to confirming the genetic background of high-, middle- and low-immune infiltration and their biological relevance. Notably, our TME classification was a platform that consistently and significantly correlated with survival and accurately accessed immunotherapy efficiency for KIRC patients.

Interestingly, the OS in Cluster A was the longest among the three clusters. Cluster B was characterized by high immune infiltration, an abundance of intratumoral CD8+ and CD4+ T-cells have been associated with high tumor grade and shorter patient survival, with higher expression of a series of immune exhaustion markers, especially CTLA4 [21]. Distinct immune status in Clusters A, B and C indicate different immunotherapy responses. CTLA-4 and PD-1/PD-L1 axis, which were targeted by nivolumab, and ipilimumab, respectively, can lead to durable responses in clinical trials [22]. Anti-LAG3 therapy was combined with anti-PD-1 therapy improving progression-free survival (47.7% vs 36.0% at 12 months, P=0.0055) in melanoma [23]. Anti-TIM-3 therapy was also confirmed efficiently (partial response & disease stability) in non-small cell lung cancer patients who were refractory to anti-PD-1 [24]. Multiple authoritative algorithms were adopted to predict immunotherapy response and to estimate the predictive potential of our classification based on non-apoptosis RCD. Our study employed a novel research designation to re-emphasize the importance of regulated cell death for immunotherapy.

The riskscore model is a robust biomarker for predicting clinical outcomes and guiding rational and effective immunotherapy. The model was constructed based on the expression of SORBS2, C1RL and GABBR1. The SORBS2, considered as Arg/c-Abl kinase binding protein 2 (ARGBP2), is an adapter protein that could interact with multiple actin regulatory proteins, including Arg, c-Cbl and Pyk2, which were enrolled in cell adhesion molecules and regulators and effectors of small GTPases [25]. Furthermore, SORBS2 was widely discovered to be involve in the process of mediating miRNA to regulate cell death [26-29]. C1RL protein, which is homologous to C1r, is considered the active form of serine hydrolase [30]. Reportedly, following ligand recognition, the binding of C1s to C1r and C1q triggers the activation of the classical complement pathway [31]. Membrane pores caused by the complement system could facilitate regulated cell death [32]. Our analyses also showed a positive correlation between the C1RL and regulated cell death (Figure S4D). GABA B type receptor (GABBR1) is a metabotropic receptor for the primary inhibitory neurotransmitter gamma-aminobutyric acid

(GABA). GABBR1 was reported to promote the growth and proliferation of hepatocellular carcinoma and cholangiocarcinoma [33, 34]. In contrast, GABBR1 can act as a tumor promoter to enhance the ability of migration and invasion of renal cancer [35]. It has been reported that GABA is involved in the regulation of mitophagy through endogenous metabolites [36]. Alternatively, programmed cell death was reported to be enhanced by the NKCC1-mediated GABA signaling [37], which further showed the profound relevance between GABBR1 and regulated cell death.

Nevertheless, there are many several essential limitations in our research. First for being restricted by the number of samples that were analyzed, our results may not represent the tumor microenvironment of physical condition. Second, the weaknesses within the bioinformatical analysis enslaved our inquiry into the exquisite machinery. Finally, conclusions demonstrated through statistical analysis were preliminary without verification by experiments. Generally speaking, by identifying various immune and non-apoptosis RCD phenotypes of kidney tumors and enabling personalized cancer biomarkers, a novel perspective was provided to dissect the heterogeneity of TME, and contributed to the identification of personalized tumor therapeutic targets for KIRC.

Conclusions

Three TME associated subtypes associated with clinical outcomes of KIRC patients were identified and the immunotherapy response was accurately predicted. The riskscore model could be a prognostic marker and help interpret the responses of KIRC to immunotherapies, providing new strategies for treating cancers.

Disclosure of conflict of interest

None.

Address correspondence to: Drs. Jiawu Wang and Qing Jiang, Department of Urology, The Second Affiliated Hospital of Chongqing Medical University, No.1 Yixueyuan Rd, Yuzhong District, Chongqing, China. Tel: +86-13629716945; E-mail: wangjiawu19850806@126.com (JWW); Tel: +86-135-08346066; E-mail: jq001002@sina.com (QJ)

References

[1] Kornauth C, Pemovska T, Vladimer GI, Bayer G, Bergmann M, Eder S, Eichner R, Erl M, Esterbauer H, Exner R, Felsleitner-Hauer V, Forte M, Gaiger A, Geissler K, Greinix HT, Gstöttner W, Hacker M, Hartmann BL, Hauswirth AW, Heinemann T, Heintel D, Hoda MA, Hopfinger G, Jaeger U, Kazianka L, Kenner L, Kiesewetter B, Krall N, Krajnik G, Kubicek S, Le T, Lubowitzki S, Mayerhoefer ME, Menschel E, Merkel O, Miura K, Müllauer L, Neumeister P, Noesslinger T, Ocko K, Öhler L, Panny M, Pichler A, Porpaczy E, Prager GW, Raderer M, Ristl R, Ruckser R, Salamon J, Schiefer AI, Schmolke AS, Schwarzinger I, Selzer E, Sillaber C, Skrabs C, Sperr WR, Srndic I, Thalhammer R, Valent P, van der Kouwe E, Vanura K, Vogt S, Waldstein C, Wolf D, Zielinski CC, Zojer N, Simonitsch-Klupp I, Superti-Furga G, Snijder B and Staber PB. Functional precision medicine provides clinical benefit in advanced aggressive hematologic cancers and identifies exceptional responders. Cancer Discov 2022; 12: 372-387.

[2] Riazalhosseini Y and Lathrop M. Precision medicine from the renal cancer genome. Nat Rev Nephrol 2016; 12: 655-666.

[3] Kumar-Sinha C and Chinnaiyan AM. Precision oncology in the age of integrative genomics. Nat Biotechnol 2018; 36: 46-60.

[4] Bagaev A, Kotlov N, Nomie K, Svekolkin V, Gafurov A, Isaeva O, Osokin N, Kozlov I, Frenkel F, Gancharova O, Almog N, Tsiper M, Ataullakhanov R and Fowler N. Conserved pan-cancer microenvironment subtypes predict response to immunotherapy. Cancer Cell 2021; 39: 845-865, e7.

[5] Braun DA, Street K, Burke KP, Cookmeyer DL, Denize T, Pedersen CB, Gohil SH, Schindler N, Pomerance L, Hirsch L, Bakouny Z, Hou Y, Forman J, Huang T, Li S, Cui A, Keskin DB, Steinharter J, Bouchard G, Sun M, Pimenta EM, Xu W, Mahoney KM, McGregor BA, Hirsch MS, Chang SL, Livak KJ, McDermott DF, Shukla SA, Olsen LR, Signoretti S, Sharpe AH, Irizarry RA, Choueiri TK and Wu CJ. Progressive immune dysfunction with advancing disease stage in renal cell carcinoma. Cancer Cell 2021; 39: 632-648, e8.

[6] Wang G, Xie L, Li B, Sang W, Yan J, Li J, Tian H, Li W, Zhang Z, Tian Y and Dai Y. A nanounit strategy reverses immune suppression of exosomal PD-L1 and is associated with enhanced ferroptosis. Nat Commun 2021; 12: 5733.

[7] Wang Q, Wang Y, Ding J, Wang C, Zhou X, Gao W, Huang H, Shao F and Liu Z. A bioorthogonal system reveals antitumour immune function of pyroptosis. Nature 2020; 579: 421-426.

[8] Kroemer G, Galluzzi L, Vandenabeele P, Abrams J, Alnemri ES, Baehrecke EH, Blagosklonny MV, El-Deiry WS, Golstein P, Green DR, Hengartner M, Knight RA, Kumar S, Lipton SA, Malorni W, Nunez G, Peter ME, Tschopp J, Yuan J, Piacentini M, Zhivotovsky B and Melino G.

Classification of cell death: recommendations of the Nomenclature Committee on Cell Death 2009. Cell Death Differ 2009; 16: 3-11.
[9] Liu Y and Levine B. Autosis and autophagic cell death: the dark side of autophagy. Cell Death Differ 2015; 22: 367-376.
[10] Liberzon A, Subramanian A, Pinchback R, Thorvaldsdottir H, Tamayo P and Mesirov JP. Molecular signatures database (MSigDB) 3.0. Bioinformatics 2011; 27: 1739-1740.
[11] Bindea G, Mlecnik B, Tosolini M, Kirilovsky A, Waldner M, Obenauf AC, Angell H, Fredriksen T, Lafontaine L, Berger A, Bruneval P, Fridman WH, Becker C, Pages F, Speicher MR, Trajanoski Z and Galon J. Spatiotemporal dynamics of intratumoral immune cells reveal the immune landscape in human cancer. Immunity 2013; 39: 782-795.
[12] Zeng D, Wu J, Luo H, Li Y, Xiao J, Peng J, Ye Z, Zhou R, Yu Y, Wang G, Huang N, Wu J, Rong X, Sun L, Sun H, Qiu W, Xue Y, Bin J, Liao Y, Li N, Shi M, Kim KM and Liao W. Tumor microenvironment evaluation promotes precise checkpoint immunotherapy of advanced gastric cancer. J Immunother Cancer 2021; 9: e002467.
[13] Aggen DH, Drake CG and Rini BI. Targeting PD-1 or PD-L1 in metastatic kidney cancer: combination therapy in the first-line setting. Clin Cancer Res 2020; 26: 2087-2095.
[14] Valero C, Lee M, Hoen D, Wang J, Nadeem Z, Patel N, Postow MA, Shoushtari AN, Plitas G, Balachandran VP, Smith JJ, Crago AM, Long Roche KC, Kelly DW, Samstein RM, Rana S, Ganly I, Wong RJ, Hakimi AA, Berger MF, Zehir A, Solit DB, Ladanyi M, Riaz N, Chan TA, Seshan VE and Morris LGT. The association between tumor mutational burden and prognosis is dependent on treatment context. Nat Genet 2021; 53: 11-15.
[15] Koren E and Fuchs Y. Modes of regulated cell death in cancer. Cancer Discov 2021; 11: 245-265.
[16] Chen DS and Mellman I. Elements of cancer immunity and the cancer-immune set point. Nature 2017; 541: 321-330.
[17] Anderton H, Wicks IP and Silke J. Cell death in chronic inflammation: breaking the cycle to treat rheumatic disease. Nat Rev Rheumatol 2020; 16: 496-513.
[18] Mazlo A, Jenei V, Burai S, Molnar T, Bacsi A and Koncz G. Types of necroinflammation, the effect of cell death modalities on sterile inflammation. Cell Death Dis 2022; 13: 423.
[19] Pasparakis M and Vandenabeele P. Necroptosis and its role in inflammation. Nature 2015; 517: 311-320.
[20] Creighton CJ, Morgan M, Gunaratne PH, Wheeler DA, Gibbs RA, Robertson AG, Chu A, Beroukhim R, Cibulskis K, Signoretti S, Vandin F, Wu HT, Raphael BJ, Verhaak RGW, Tamboli P, Torres-Garcia W, Akbani R, Weinstein JN, Reuter V, Hsieh JJ, Brannon AR, Hakimi AA, Jacobsen A, Ciriello G, Reva B, Ricketts CJ, Linehan WM, Stuart JM, Rathmell WK, Shen H, Laird PW, Muzny D, Davis C, Morgan M, Xi L, Chang K, Kakkar N, Trevino LR, Benton S, Reid JG, Morton D, Doddapaneni H, Han Y, Lewis L, Dinh H, Kovar C, Zhu Y, Santibanez J, Wang M, Hale W, Kalra D, Creighton CJ, Wheeler DA, Gibbs RA, Getz G, Cibulskis K, Lawrence MS, Sougnez C, Carter SL, Sivachenko A, Lichtenstein L, Stewart C, Voet D, Fisher S, Gabriel SB, Lander E, Beroukhim R, Schumacher SE, Tabak B, Saksena G, Onofrio RC, Carter SL, Cherniack AD, Gentry J, Ardlie K, Sougnez C, Getz G, Gabriel SB, Meyerson M, Robertson AG, Chu A, Chun HJE, Mungall AJ, Sipahimalani P, Stoll D, Ally A, Balasundaram M, Butterfield YSN, Carlsen R, Carter C, Chuah E, Coope RJN, Dhalla N, Gorski S, Guin R, Hirst C, Hirst M, Holt RA, Lebovitz C, Lee D, Li HI, Mayo M, Moore RA, Pleasance E, Plettner P, Schein JE, Shafiei A, Slobodan JR, Tam A, Thiessen N, Varhol RJ, Wye N, Zhao Y, Birol I, Jones SJM, Marra MA, Auman JT, Tan D, Jones CD, Hoadley KA, Mieczkowski PA, Mose LE, Jefferys SR, Topal M, Liquori C, Turman YJ, Shi Y, Waring S, Buda E, Walsh J, Wu J, Bodenheimer T, Hoyle AP, Simons JV, Soloway M, Balu S, Parker JS, Hayes DN, Perou CM, Kucherlapati R, Park P, Shen H, Triche T Jr, Weisenberger DJ, Lai PH, Bootwalla MS, Maglinte DT, Mahurkar S, Berman BP, Van den Berg DJ, Cope L, Baylin SB, Laird PW, Creighton CJ, Wheeler DA, Getz G, Noble MS, DiCara D, Zhang H, Cho J, Heiman DI, Gehlenborg N, Voet D, Mallard W, Lin P, Frazer S, Stojanov P, Liu Y, Zhou L, Kim J, Lawrence MS, Chin L, Vandin F, Wu HT, Raphael BJ, Benz C, Yau C, Reynolds SM, Shmulevich I, Verhaak RGW, Torres-Garcia W, Vegesna R, Kim H, Zhang W, Cogdell D, Jonasch E, Ding Z, Lu Y, Akbani R, Zhang N, Unruh AK, Casasent TD, Wakefield C, Tsavachidou D, Chin L, Mills GB, Weinstein JN, Jacobsen A, Brannon AR, Ciriello G, Schultz N, Hakimi AA, Reva B, Antipin Y, Gao J, Cerami E, Gross B, Aksoy BA, Sinha R, Weinhold N, Sumer SO, Taylor BS, Shen R, Ostrovnaya I, Hsieh JJ, Berger MF, Ladanyi M, Sander C, Fei SS, Stout A, Spellman PT, Rubin DL, Liu TT, Stuart JM, Sam N, Paull EO, Carlin D, Goldstein T, Waltman P, Ellrott K, Zhu J, Haussler D, Gunaratne PH, Xiao W, Shelton C, Gardner J, Penny R, Sherman M, Mallery D, Morris S, Paulauskis J, Burnett K, Shelton T, Signoretti S, Kaelin WG, Choueiri T, Atkins MB, Penny R, Burnett K, Mallery D, Curley E, Tickoo S, Reuter V, Rathmell WK, Thorne L, Boice L, Huang M, Fisher JC, Linehan WM, Vocke CD, Peterson J, Worrell R, Merino MJ, Schmidt LS, Tamboli P, Czerniak BA, Aldape KD, Wood CG,

Boyd J, Weaver J, Iacocca MV, Petrelli N, Witkin G, Brown J, Czerwinski C, Huelsenbeck-Dill L, Rabeno B, Myers J, Morrison C, Bergsten J, Eckman J, Harr J, Smith C, Tucker K, Zach LA, Bshara W, Gaudioso C, Morrison C, Dhir R, Maranchie J, Nelson J, Parwani A, Potapova O, Fedosenko K, Cheville JC, Thompson RH, Signoretti S, Kaelin WG, Atkins MB, Tickoo S, Reuter V, Linehan WM, Vocke CD, Peterson J, Merino MJ, Schmidt LS, Tamboli P, Mosquera JM, Rubin MA, Blute ML, Rathmell WK, Pihl T, Jensen M, Sfeir R, Kahn A, Chu A, Kothiyal P, Snyder E, Pontius J, Ayala B, Backus M, Walton J, Baboud J, Berton D, Nicholls M, Srinivasan D, Raman R, Girshik S, Kigonya P, Alonso S, Sanbhadti R, Barletta S, Pot D, Sheth M, Demchok JA, Davidsen T, Wang Z, Yang L, Tarnuzzer RW, Zhang J, Eley G, Ferguson ML, Shaw KRM, Guyer MS, Ozenberger BA and Sofia HJ; Cancer Genome Atlas Research Network and Anal Working Group. Comprehensive molecular characterization of clear cell renal cell carcinoma. Nature 2013; 499: 43-49.

[21] Diaz-Montero CM, Rini BI and Finke JH. The immunology of renal cell carcinoma. Nat Rev Nephrol 2020; 16: 721-735.

[22] Sharma P and Allison JP. The future of immune checkpoint therapy. Science 2015; 348: 56-61.

[23] Simpson TR, Li F, Montalvo-Ortiz W, Sepulveda MA, Bergerhoff K, Arce F, Roddie C, Henry JY, Yagita H, Wolchok JD, Peggs KS, Ravetch JV, Allison JP and Quezada SA. Fc-dependent depletion of tumor-infiltrating regulatory T cells co-defines the efficacy of anti-CTLA-4 therapy against melanoma. J Exp Med 2013; 210: 1695-1710.

[24] Wolf Y, Anderson AC and Kuchroo VK. TIM3 comes of age as an inhibitory receptor. Nat Rev Immunol 2020; 20: 173-185.

[25] Zhao L, Wang W, Huang S, Yang Z, Xu L, Yang Q, Zhou X, Wang J, Shen Q, Wang C, Le X, Feng M, Zhou N, Lau WB, Lau B, Yao S, Yi T, Wang X, Zhao X, Wei Y and Zhou S. The RNA binding protein SORBS2 suppresses metastatic colonization of ovarian cancer by stabilizing tumor-suppressive immunomodulatory transcripts. Genome Biol 2018; 19: 35.

[26] An J, Wang H, Ma X, Hu B, Yan Y, Yan Y and Su Z. Musk ketone induces apoptosis of gastric cancer cells via downregulation of sorbin and SH3 domain containing 2. Mol Med Rep 2021; 23: 450.

[27] Shan B, Li JY, Liu YJ, Tang XB, Zhou Z and Luo LX. LncRNA H19 inhibits the progression of sepsis-induced myocardial injury via regulation of the miR-93-5p/SORBS2 axis. Inflammation 2021; 44: 344-357.

[28] Backsch C, Rudolph B, Steinbach D, Scheungraber C, Liesenfeld M, Haefner N, Hildner M, Habenicht A, Runnebaum IB and Duerst M. An integrative functional genomic and gene expression approach revealed SORBS2 as a putative tumour suppressor gene involved in cervical carcinogenesis. Carcinogenesis 2011; 32: 1100-1106.

[29] Wang H, Bei Y, Shen S, Huang P, Shi J, Zhang J, Sun Q, Chen Y, Yang Y, Xu T, Kong X and Xiao J. miR-21-3p controls sepsis-associated cardiac dysfunction via regulating SORBS2. J Mol Cell Cardiol 2016; 94: 43-53.

[30] McLure CA, Williamson JF, Stewart BJ, Keating PJ and Dawkins RL. Genomic analysis reveals a duplication of eight rather than seven short consensus repeats in primate CR1 and CR1L: evidence for an additional set shared between CR1 and CR2. Immunogenetics 2004; 56: 631-638.

[31] Lu J and Kishore U. C1 complex: an adaptable proteolytic module for complement and non-complement functions. Front Immunol 2017; 8: 592.

[32] Fishelson Z and Kirschfink M. Complement C5b-9 and cancer: mechanisms of cell damage, cancer counteractions, and approaches for intervention. Front Immunol 2019; 10: 752.

[33] Wang T, Huang W and Chen F. Baclofen, a GABAB receptor agonist, inhibits human hepatocellular carcinoma cell growth in vitro and in vivo. Life Sci 2008; 82: 536-541.

[34] Fava G, Marucci L, Glaser S, Francis H, De Morrow S, Benedetti A, Alvaro D, Venter J, Meininger C, Patel T, Taffetani S, Marzioni M, Summers R, Reichenbach R and Alpini G. gamma-aminobutyric acid inhibits cholangiocarcinoma growth by cyclic AMP-dependent regulation of the protein kinase A/extracellular signal-regulated kinase 1/2 pathway. Cancer Res 2005; 65: 11437-11446.

[35] Inamoto T, Azuma H, Kotake Y, Watanabe M and Katsuoka Y. Gamma-aminobutyric acid modulates invasive property in renal cancer. J Urol 2008; 179: 90.

[36] Zhang T, Liu Q, Gao W, Sehgal SA and Wu H. The multifaceted regulation of mitophagy by endogenous metabolites. Autophagy 2022; 18: 1216-1239.

[37] Blanquie O, Liebmann L, Hubner CA, Luhmann HJ and Sinning A. NKCC1-mediated GABAergic signaling promotes postnatal cell death in neocortical Cajal-Retzius cells. Cereb Cortex 2017; 27: 1644-1659.

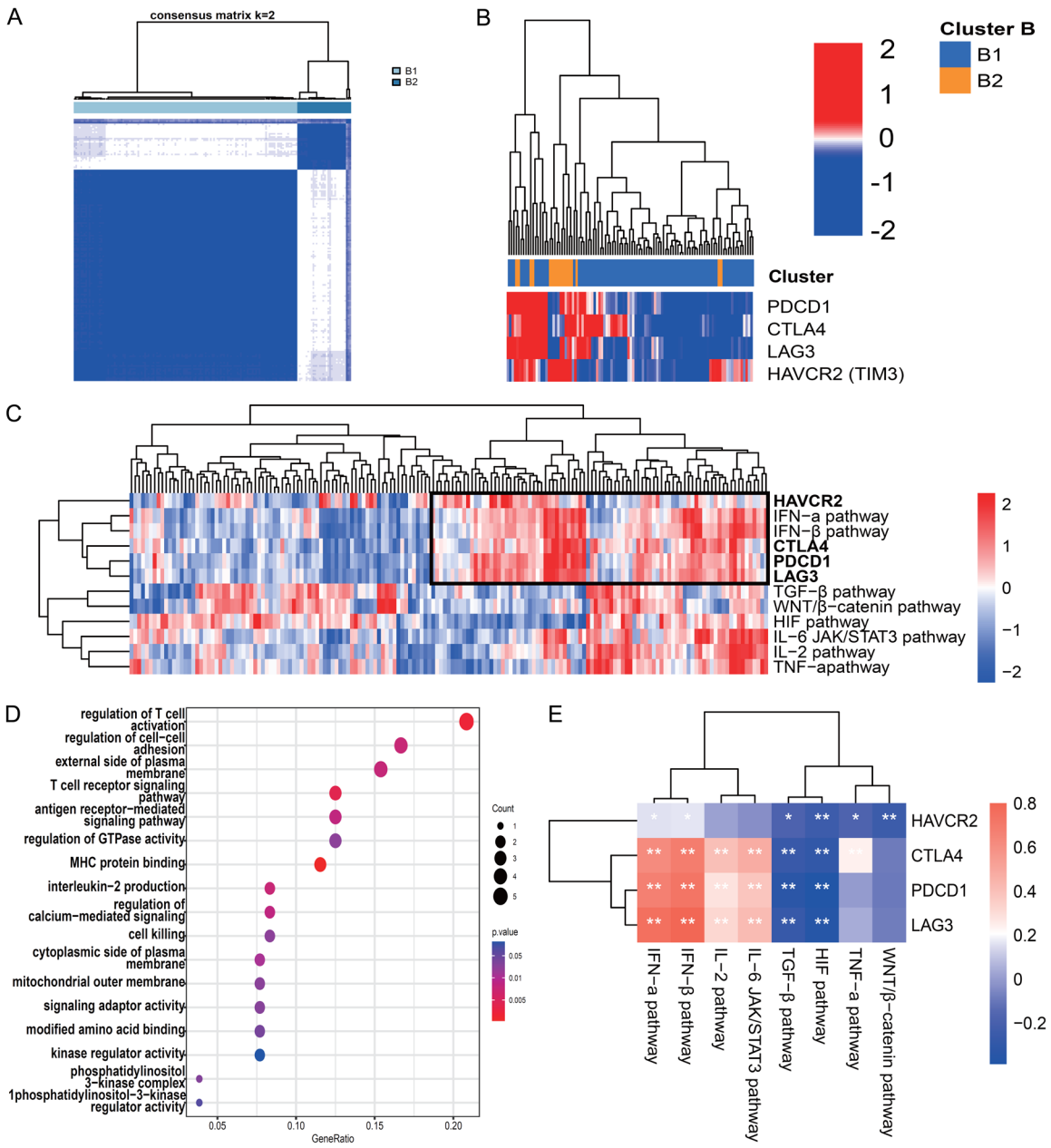

Figure S1. Upregulation of immune checkpoints in cluster B is regulated by numerous mechanisms: (A) Consensus heatmap demonstrated two robust clusters (B1, B2) based on patients in Cluster B; (B) Heatmap demonstrating expression of immune checkpoints, samples were clustered by B1 and B2, z-scores were calculated for each gens; (C) Expression levels of immune checkpints and enrichment scores of pathways each patient, those circled by boxes refer to ratings with the same expression trend; (D) Gene ontology analysis of genes correlating with immune checkpoints; (E) Heatmap showing the correlation between the enrichment of pathways and expression of immune checkpoints.

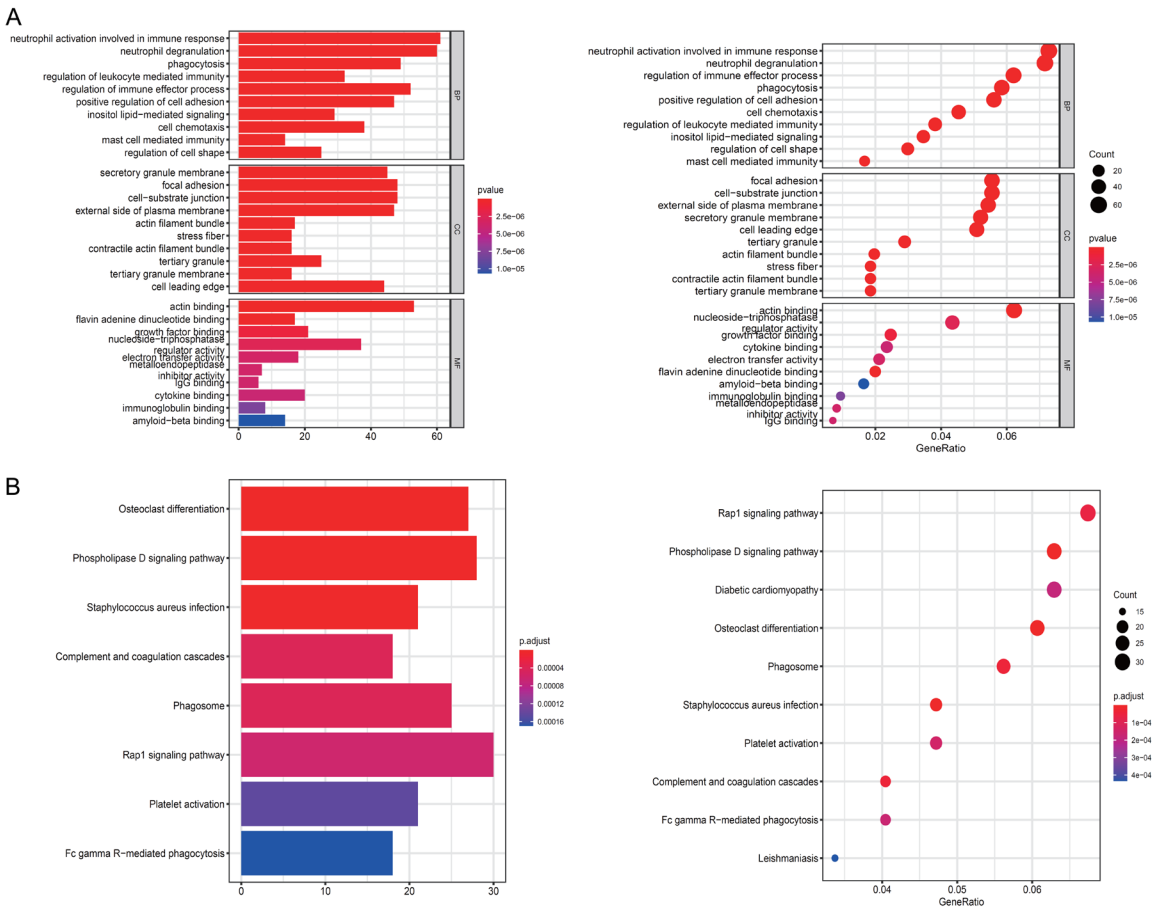

Figure S2. Enrichment analysis of phenotypes related DEGs. (A) Gene ontology enrichment analysis of phenotypes-related DEGs; (B) Kyoto Encyclopedia of Genes and Genomes enrichment analysis.

A

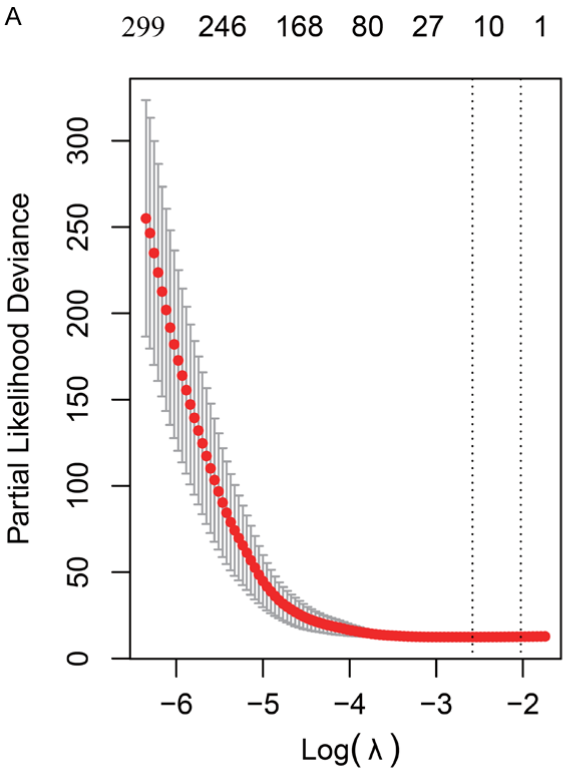

B

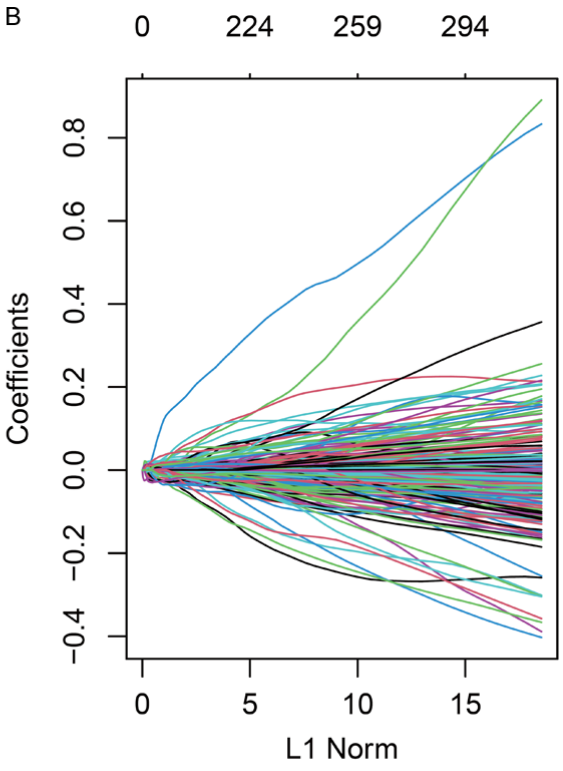

C

	pvalue	Hazard ratio
CREB3L1	<0.001	1.011(1.007−1.015)
HERC2P2	<0.001	1.058(1.038−1.080)
SERPINF1	<0.001	1.002(1.001−1.003)
TMEM132A	<0.001	1.022(1.015−1.028)
TMEM150C	<0.001	0.973(0.965−0.981)
SORBS2	<0.001	0.934(0.916−0.951)
ACADM	<0.001	0.981(0.975−0.986)
SLC27A2	<0.001	0.985(0.980−0.990)
PABPC1L	<0.001	1.018(1.012−1.023)
C1RL	<0.001	1.017(1.011−1.024)
ALDH3A2	<0.001	0.987(0.983−0.991)
GABBR1	<0.001	1.057(1.037−1.078)
EMCN	<0.001	0.982(0.976−0.987)
CEP55	<0.001	1.044(1.032−1.056)
BSPRY	<0.001	0.935(0.909−0.962)

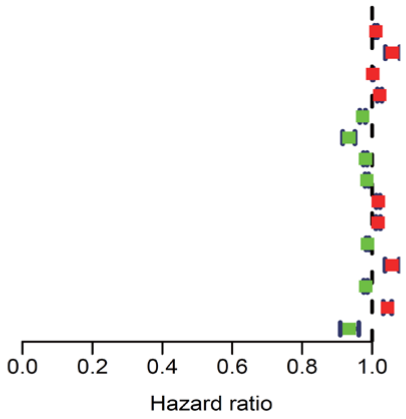

D

	pvalue	Hazard ratio
CREB3L1	0.083	1.007(0.999−1.015)
HERC2P2	0.506	1.010(0.981−1.040)
SERPINF1	0.721	1.000(0.999−1.002)
TMEM132A	0.626	0.998(0.988−1.008)
TMEM150C	0.713	0.997(0.984−1.011)
SORBS2	0.007	0.964(0.938−0.990)
ACADM	0.464	0.997(0.988−1.006)
SLC27A2	0.503	0.998(0.991−1.005)
PABPC1L	0.466	0.996(0.984−1.007)
C1RL	0.022	1.010(1.001−1.018)
ALDH3A2	0.626	0.998(0.992−1.005)
GABBR1	0.002	1.049(1.017−1.081)
EMCN	0.656	0.998(0.989−1.007)
CEP55	0.203	1.012(0.994−1.031)
BSPRY	0.139	0.982(0.958−1.006)

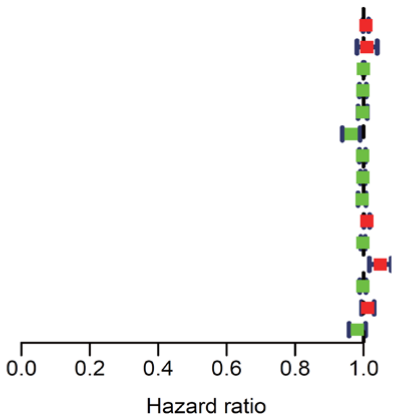

Figure S3. Identification of prognosis associated phenotypes related DEGs. (A, B) Show coefficient results derived from LASSO Cox regression algorithm; (C) Univariate cox regression analysis of genes selected from LASSO algorithm; (D) Multivariate cox regression analysis of genes selected from univariate cox regression analysis, genes marked by red squares were screened out for riskscore construction.

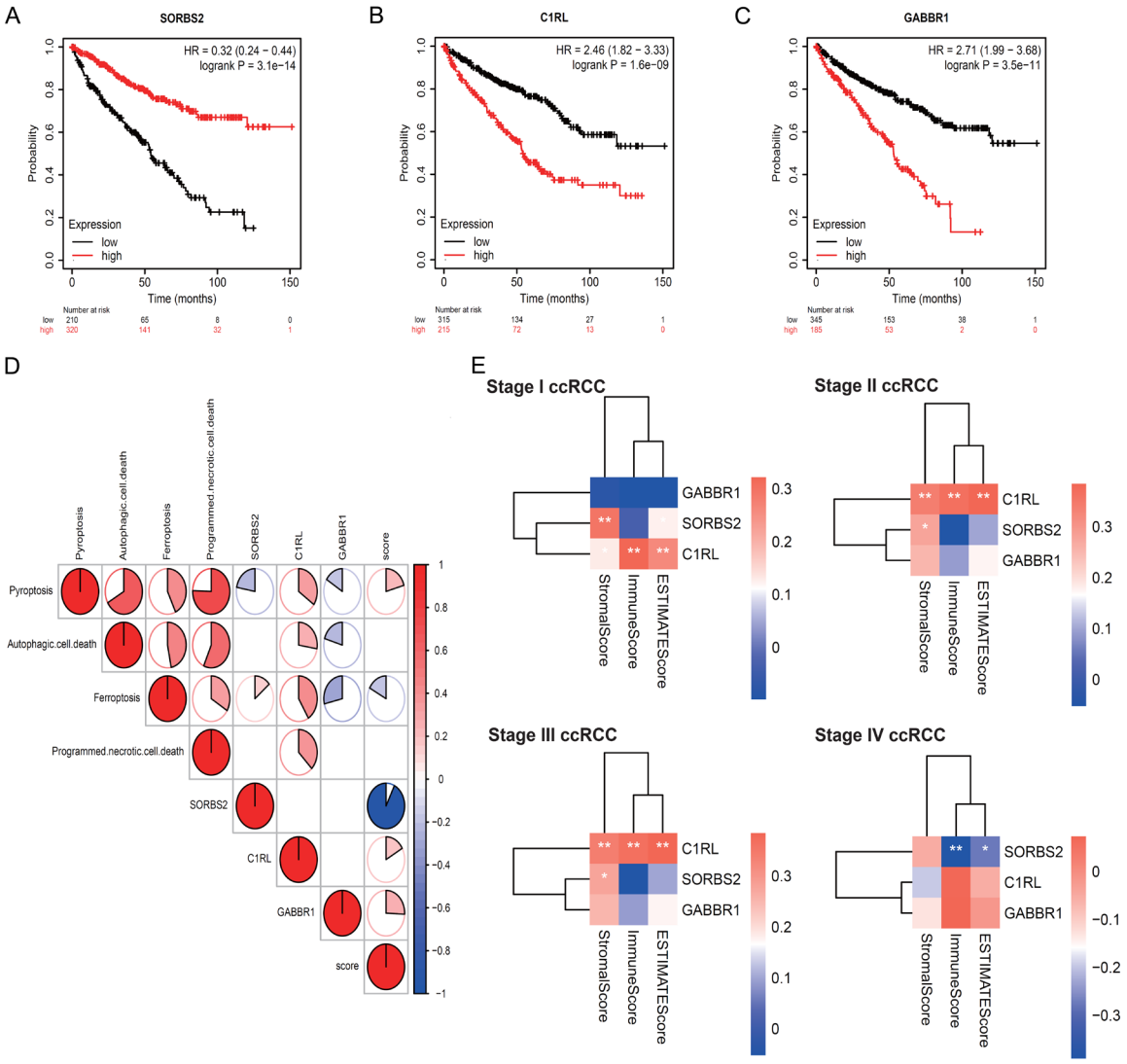

Figure S4. Survival analysis of (A) SORBS2, (B) C1RL and (C) GABBR1, (D) Intrinsic correlation of non-apoptosis RCD and candiate genes expression. The circular area suggests a *p*-value, while the colour depth represents the correlation coefficient; (E) Heatmap reveals the correlation between expression levels of SORBS2, C1RL, and GABBR1 and values of StromalScore, ImmuneScore, and ESTIMATEScore at different clinical stages of ccRCC patients, respectively. Welch's t test: *P < 0.05; **P < 0.01; ***P < 0.001.